



**HAL**  
open science

## **ZeoZeolitic germanosilicate analogue to pharmacosiderite crystallized in an acidic medium**

Guangying Fu, Qiaolin Lang, Xiaolong Liu, Haonuan Zhao, Yiqing Sun, Lei Zhao, Ahmed Omran, Peng Lu, Xiaobo Yang, Bing Yu, et al.

### ► To cite this version:

Guangying Fu, Qiaolin Lang, Xiaolong Liu, Haonuan Zhao, Yiqing Sun, et al.. ZeoZeolitic germanosilicate analogue to pharmacosiderite crystallized in an acidic medium. Green Carbon, In press, 10.1016/j.greenca.2023.11.003 . hal-04310345

**HAL Id: hal-04310345**

**<https://hal.science/hal-04310345>**

Submitted on 27 Nov 2023

**HAL** is a multi-disciplinary open access archive for the deposit and dissemination of scientific research documents, whether they are published or not. The documents may come from teaching and research institutions in France or abroad, or from public or private research centers.

L'archive ouverte pluridisciplinaire **HAL**, est destinée au dépôt et à la diffusion de documents scientifiques de niveau recherche, publiés ou non, émanant des établissements d'enseignement et de recherche français ou étrangers, des laboratoires publics ou privés.

# Zeolitic germanosilicate analogue to pharmacosiderite crystallized in an acidic medium

Guangying Fu,<sup>a</sup> Qiaolin Lang,<sup>a</sup> Xiaolong Liu,<sup>a,b</sup> Haonuan Zhao,<sup>c</sup> Yiqing Sun,<sup>a,b</sup> Lei Zhao,<sup>a</sup> Ahmed Omran,<sup>c</sup> Peng Lu,<sup>a</sup> Xiaobo Yang,<sup>\*a</sup> Bing Yu,<sup>\*b</sup> Valentin Valtchev<sup>\*a,c</sup>

- a. The ZeoMat Group, Qingdao Institute of Bioenergy and Bioprocess Technology, Chinese Academy of Science, Laoshan District, CN-266101 Qingdao, China. E-mail: [yangxb@qibebt.ac.cn](mailto:yangxb@qibebt.ac.cn).
- b. College of Chemistry and Chemical Engineering, Qingdao University, CN-266071 Qingdao, China. E-mail: [yubing198@qdu.edu.cn](mailto:yubing198@qdu.edu.cn).
- c. Normandie University, ENSICAEN, UNICAEN, CNRS, Laboratoire Catalyse et Spectrochimie, F-14000 Caen, France. E-mail: [valentin.valtchev@ensicaen.fr](mailto:valentin.valtchev@ensicaen.fr).

## Abstract

Zeolites are typically synthesized in alkaline or fluoride-containing near-neutral media. Sophisticated organic structure-directing agents have been investigated for such systems with the aim of discovering materials with unprecedented structures and properties for novel technical applications. In contrast, zeolite crystallization in strongly acidic media has yet to be explored. This study demonstrates that a zeolitic silicate phase crystallizes from acidic gels using trimethylamine as an organic additive with the composition 1 SiO<sub>2</sub>: 0.3 TMA: 0.3 HCl: 0.15 HF: 55 H<sub>2</sub>O: (0.1-0.4) GeO<sub>2</sub>. This phase has an interrupted four-connected framework analog to the octahedron/tetrahedron-mixed framework of the mineral family pharmacosiderite. In comparison to the pharmacosiderite-type HK<sub>3</sub>(Ge<sub>7</sub>O<sub>16</sub>)(H<sub>2</sub>O)<sub>4</sub>, the four GeO<sub>6</sub>-octahedra forming the central [HGe<sub>4</sub>O<sub>4</sub>O<sub>12</sub>]-cluster are replaced by four SiO<sub>4</sub>-tetrahedra in a [Si<sub>4</sub>O<sub>6</sub>(OH)<sub>2.89</sub>]-unit in the new phase. However, the structure is distorted and may contain connectivity and point defects; thus, healing by the occasional incorporation of GeO<sub>6</sub>-units is necessary. The refined unit cell has a cubic symmetry, space group P-43m (#215), with a = 7.7005(1) Å. Acidic-medium synthesis is a useful way to find new zeolites that move in a fundamentally different direction from sophisticated organic structure-directing agents.

**Keywords:** Zeolite synthesis in acidic medium, new germanosilicate zeolite, 4-

connected analogue of pharmacosiderite, structure analysis, structure-directing agents

## **Introduction**

Zeolites are crystalline microporous silicates with framework structures constructed by corner-sharing  $\text{SiO}_4$ -tetrahedra with isomorphous substitutions of heteroatoms, such as Al and other metal ions, for a portion of Si. They are the most important sorbents, ion exchangers, and catalysts in oil refinery and petrochemical industries [1-3].

Nowadays, society undergoes an energy transition from fossil fuels to renewables, aiming to reduce  $\text{CO}_2$  emissions and “green” utilization of carbon resources. Zeolites contribute to the energy transition by providing energy- and material-efficient processes in the fossil energy industry and developing new technologies for producing chemicals from  $\text{C}_1$  and other low hydrocarbons, processing biomass, and recycling plastics [4].

The emerging applications of zeolites in the processing of renewable feedstocks, air protection, medicine delivery, and as advanced functional materials require that zeolites work under conditions remarkably different from their conventional applications [5, 6]. The demands of zeolitic materials with new properties are therefore exerted, such as larger micropores, predictable hydrophilicity/hydrophobicity, and reliable structural stability. Much of the current synthetic research has focused on exploring sophisticated organic structure-directing agents (SDA) that facilitate the crystallization of zeolites with unknown frameworks [7-10]. Recent successes in such explorations are, for example, the three-dimensional extra-large pore (16-MR) zeolite ZEO-1 crystallized with a substituted phosphonium ion as the SDA [11], and ITQ-56 (22-MR) crystallized using a modified memantine SDA [12].

Despite intensive synthesis research, there is still a large gap between the known zeolite structures and the hypothetical number of energetically favored four-connected frameworks [13, 14]. The International Zeolite Association has recognized less than 260 unique framework topologies thus far [15], whereas over 10 million energetically optimized virtual structures have been predicted, for example, by Treacy and Foster [16]. The fact that this large gap has not

been overcome in decades may imply a limitation in the hydrothermal crystallization system applied in zeolite synthesis. Therefore, in addition to the exploration of new SDA, further expansion of the field of chemistry should be considered.

We have recently demonstrated that high-silica zeolite crystallization can occur in a strongly acidic fluoride medium [17-21]. Fundamentally different from the traditional alkaline hydrothermal crystallization system [22, 23] and the near-neutral “fluoride route” [24, 25], acidic-medium synthesis enables the use of chemical compositions and SDA molecules that are only feasible in acidic conditions. An example of the SDAs is urotropine, which is a strongly hydrophilic molecule that does not interact with silicates in basic systems. However, in acidic media, the protonated urotropine cation becomes a selective and robust SDA for the crystallization of the high-silica MTN-type zeolite [20].

This study illustrates that a new zeolitic crystalline phase can crystallize in an acidic medium even with a simple amine molecule, trimethylamine (TMA), as an organic additive. To date, acidic medium synthesis has been a nearly unexplored field, and many potential SDA molecules remain untested. Thus, studying simple organic additives in the new acidic chemistry may provide a practical complement to the exploration of sophisticated SDAs in conventional systems. Details of the synthesis and structural analysis of the TMA-directed product are presented in the sections below.

## **Experimental**

### **Synthesis**

The chemical reagents were used as purchased: Ludox AS-40 (Sigma Aldrich, 40% SiO<sub>2</sub> aq., Si/Na >200), GeO<sub>2</sub> (Aladdin, 99.99%), trimethylamine hydrochloride (TMA·HCl, Aladdin, 98%), hydrofluoric acid (AR, 40% aq.), and deionized water.

For each synthetic batch, TMA·HCl of the amount according to Table 1 was dissolved in HF and water. Ludox and GeO<sub>2</sub> were then added while stirring. The mixture was then stirred at room temperature for 24 h. The crystallization

was performed in Teflon-lined autoclaves at 160 °C under tumbling at 15 rpm for 23 days. The recovered solid product was washed thoroughly with water and dried at 80 °C in air.

Caution: Hydrofluoric acid is a hazardous chemical that is toxic and irritative to the human skin, eyes, and respiratory system. They are also corrosive to metals and glass. Caution must be taken to handle it properly according to the relevant safety protocols, including wearing protective clothing, gloves, eyeglasses, and masks. The gel preparation and further treatments were performed in fume hoods in Teflon vials.

Table 1: Synthetic recipes and powder XRD detected product phases

Sample #	Recipe	Gel pH	Crystallization	XRD phase	XRF Ge/Si	XRF Na/Ge <sup>c</sup>
GSQ0	1 SiO <sub>2</sub> : 0.3 R: 0.15 HF: 55 H <sub>2</sub> O: 0 GeO <sub>2</sub> <sup>a</sup>	3.2	160°C, 30 days	Amorphous gel	/	/
GSQ1	1 SiO <sub>2</sub> : 0.3 R: 0.15 HF: 55 H <sub>2</sub> O: 0.1 GeO <sub>2</sub>	3.2	160°C, 23 days	GSQ <sup>b</sup> + Amorph.	0.05	0.7
GSQ2	1 SiO <sub>2</sub> : 0.3 R: 0.15 HF: 55 H <sub>2</sub> O: 0.2 GeO <sub>2</sub>	3.2	160°C, 23 days	GSQ + less amorph.	0.06	0.8
GSQ3	1 SiO <sub>2</sub> : 0.3 R: 0.15 HF: 55 H <sub>2</sub> O: 0.3 GeO <sub>2</sub>	3.2	160°C, 23 days	GSQ + less amorph.	0.10	0.6
GSQ4	1 SiO <sub>2</sub> : 0.3 R: 0.15 HF: 55 H <sub>2</sub> O: 0.4 GeO <sub>2</sub>	3.2	160°C, 23 days	GSQ + least amorph.	0.15	0.5

<sup>a</sup> R = trimethylamine hydrochloride (TMA·HCl).

<sup>b</sup> See details about GSQ in Results and Discussions/Structure Analysis.

<sup>c</sup> After ion-exchange with NaCl.

## Characterization

Powder X-ray diffraction was performed on a Rigaku SmartLab diffractometer using Cu K $\alpha$  radiation at 40 kV and 150 mA. A 1D D/teX Ultra250 detector equipped with a series of linearly aligned X-ray intensity-sensing units was used to collect the diffractions in continuous scans in the theta-theta geometry at  $2\theta = 5^\circ - 50^\circ$  for phase identification.

*In-situ* XRD patterns at higher temperatures (HT) up to 1300 °C of selected samples were recorded using a HT chamber with Be windows. The sample was exposed to ambient air with 50% relative humidity and heated at a rate of 5 °C/min at 50 °C steps. At each step, the temperature was maintained for 5 min for XRD recording. A platinum plate was used as the sample holder.

High-resolution XRD data were recorded using a single point of the D/teX detector (0D mode) in steps of 0.01° from  $2\theta = 5^\circ$  to 120°.

The SEM images of the powder samples were obtained using a Hitachi S-4800 Scanning Electron Microscope equipped with a cold-field emission gun operating at 5 kV. The samples were deposited on carbon sheets and inspected without coating.

TG/DTA analysis was performed using a Rigaku TG-DTA8122 microbalance with ca. 10 mg of zeolite powder against  $\alpha$ -Al<sub>2</sub>O<sub>3</sub> in a 50 ml/min reconstituted airflow at a heating rate of 10 °C/min.

<sup>29</sup>Si MAS NMR experiments were performed using a Bruker AVANCE III 600 spectrometer at a resonance frequency of 119.2 MHz. The spectra with high-power proton decoupling were recorded on a 4 mm probe with a spinning rate of 10 kHz, a  $\pi/4$  pulse length of 2.6  $\mu$ s, and a recycle delay of 60 s. The chemical shifts of <sup>29</sup>Si are referred to TMS.

FTIR spectra were recorded upon KBr pellets using Bruker Vertex 70V Spectrometer at a spectral resolution of 4 cm<sup>-1</sup>. The equipment, including the sample chamber, was evacuated to < 1 hPa.

### **Rietveld refinement**

Indexing of the high-resolution XRD of the sample GSQ4 was performed using the TREOR [26] package built-in Rigaku SmartLab. Pawley intensity extraction and space group assignment were performed using the EXPO software [27]. The initial structure was prepared using Shelx [28]. Rietveld refinement was performed using GSAS-II [29]. The background was fitted with a shifted Chebychev function using 21 parameters. The peak profile was fitted using a pseudo-Voigt function with one additional parameter (SH/L) for the asymmetrical shape [30]. Soft constraints were applied to Si-O distances for 1.61 Å, with 0.1 tolerances and weight factors of 1 [31-33]. In the 2 $\theta$  range of 7–118°, there are 11101 observations and 95 reflections applied to 40 variables.

### **Ion-exchange experiment**

A sample of GSQ4 powder (0.5 g) (Table 1) was soaked in 10 mL of 0.2 M NaCl solution in a sealed polypropylene (PP) bottle at 80 °C overnight. Thereafter, the solid was recovered through filtration, washed with plenty amounts of water, and dried at 80 °C in air. The dried sample was subjected to XRF to analyze the Na<sup>+</sup> content.

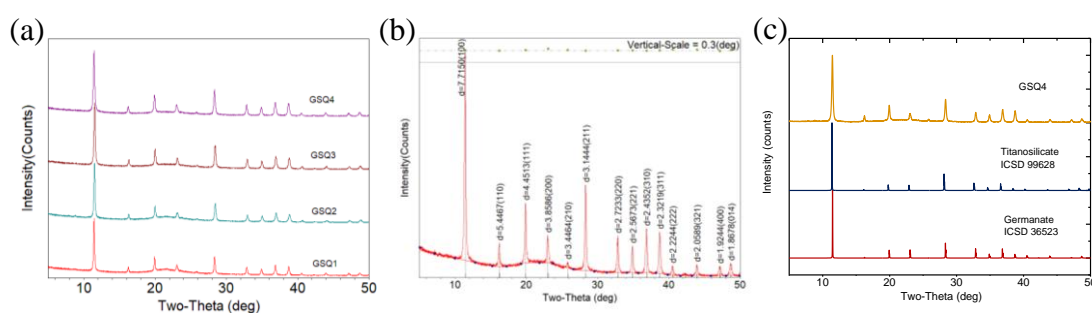
## Results and discussion

### Synthesis and phase identification

Out of the recipes with increasing Ge amounts in the initial gels composed of TMA·HCl, HF, and silica sol, as listed in Table 1, a crystalline phase has been obtained, which we tentatively name as GSQ. GSQ denotes GermanoSilicate Qingdao. The powder XRD patterns of the products are shown in Figure 1a. The observed peaks are readily indexed to a cubic unit cell with  $a = 7.7 \text{ \AA}$  (Figure 1b). However, an amorphous phase presents, which is recognizable as a broad bulge at approximately  $2\theta = 22^\circ$ . The amount of the amorphous impurity decreases with increasing Ge content in the initial gels. Another minor crystalline phase may be present, as indicated by the very weak reflections at  $2\theta = 7.9$  and  $8.8^\circ$ , which are unindexed.

The XRF analysis of the products reveals that the Ge/Si ratios increase with the Ge/Si ratios in the initial gels, but a linear relationship does not appear. In general, less than half of the introduced Ge is found in the products (Table 1). The products do not have a fixed chemical stoichiometry respect to the Ge/Si ratio.

The XRD patterns show great similarity to the material family of mineral pharmacosiderites (Figure 1c). However, pharmacosiderite has an octahedron/tetrahedron-mixed framework with a fixed stoichiometry of O/T = 4/3.[34] For our GSQ1-GSQ4 samples, the highest Ge/Si ratio is 0.15, which is far below 4/3. In addition, Si hardly forms an octahedron with oxygen atoms. Therefore, GSQ is unlikely to be pharmacosiderite. This difference is discussed below, along with the

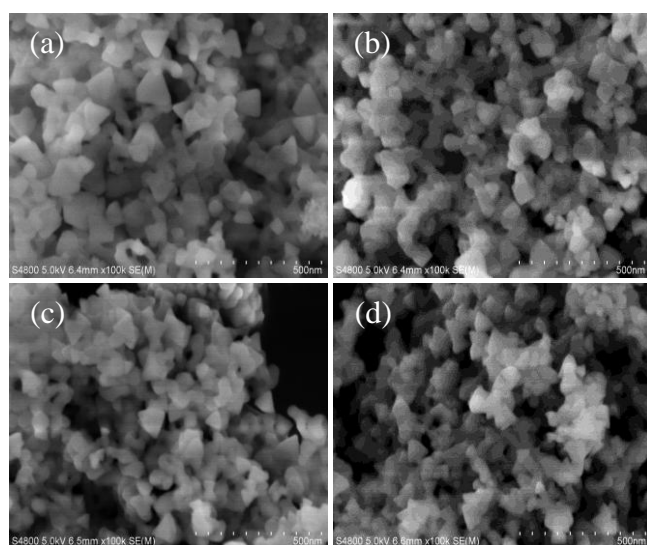


results of the structural analysis.

**Figure 1:** Powder XRD patterns of the hydrothermal crystallization products from

gels with increasing Ge/Si ratios as in Table 1 (a); the indexing results of the crystalline phase in a cubic unit cell with  $a = 7.7 \text{ \AA}$  (b); and the comparison with simulated patterns of two pharmacosiderites, a titanosilicate, and a germanate (c).

The SEM images in Figure 2 show that GSQ samples consist of small crystallites of the octahedral shape with edge lengths ranging from a few tens to 100 nm. The octahedral shape is frequently observed in crystals with cubic symmetry, that is, the



XRD indexing and SEM results are consistent.

**Figure 2:** SEM images of the hydrothermal crystallization products GSQ1-GSQ4 (a-d) from gels with increasing Ge/Si ratios as in Table 1.

TG/DTA and *in-situ* XRD reveal a series of phase transitions of GSQ upon heating in air (Figure 3). Sample GSQ4 (Table 1) was chosen as a representative because it has the least amount of amorphous impurity. From room temperature to above 200 °C, the sample loses ca. 14 wt% of its weight in seemingly two endothermic dehydration processes: a slow step up to ca. 180 °C, corresponding to the desorption of adsorbed water, and another sharp step that consumes significant heat, corresponding to an abrupt release of crystal water. The crystalline structure of GSQ collapses into an amorphous phase when the dehydration completes. From ca. 650 °C, corresponding to the exothermic peak in DTA, the amorphous material crystallizes mainly into cristobalite and releases heat. Above 1200 °C, cristobalite collapses, and an

endothermic peak was observed in DTA. Another minor crystalline phase appears at 900 °C and 1000 °C, where DTA shows an exothermic signal followed by an endothermic signal. This phase disappears at 1100 °C. One more recrystallization process is observable in the DTA trace at ca. 1350 °C, but is already beyond the range of the XRD experiment. The crystalline GSQ phase exists only below ca. 200 °C at the hydrated state.

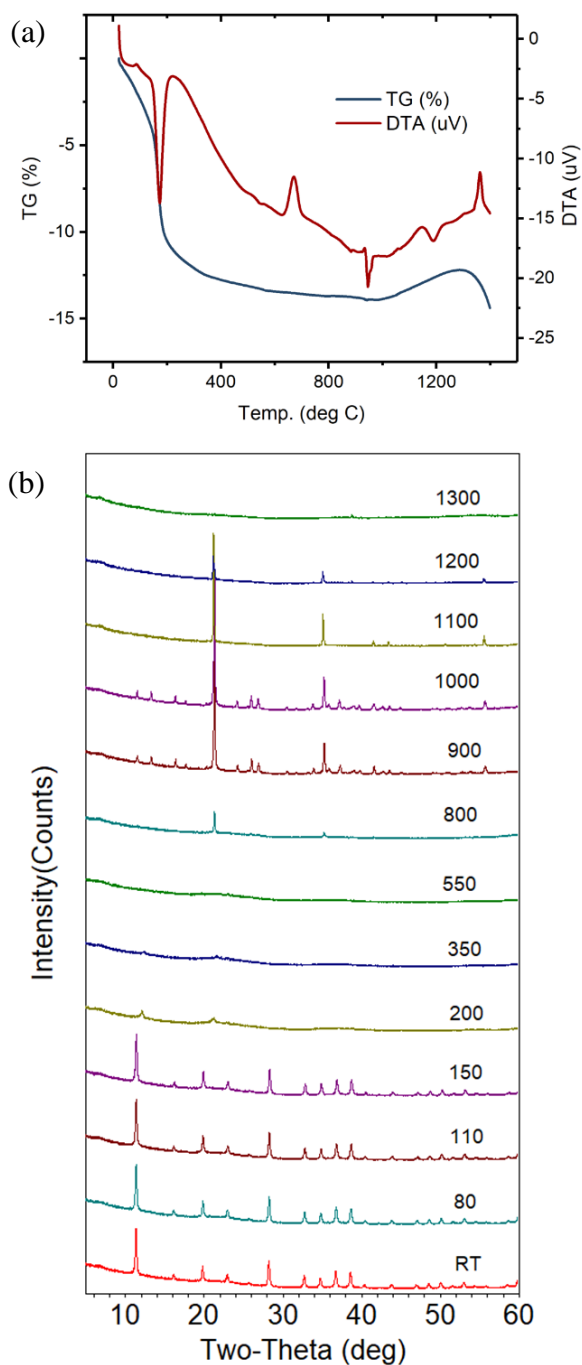


**Figure 3:** Phase transitions of GSQ upon heating in air, as revealed by TG/DTA (a) and *in-situ* XRD (b).

The product does not occlude the organic TMA additive used in the synthesis. Otherwise, one would expect the corresponding weight losses for its decomposition and combustion in the 200–600 °C temperature range, with significant heat effects. CHN analysis has not revealed any meaningful numbers for either element above the noise level (Table S5). It appears that TMA acts as a pH buffer or rheological modifier during hydrothermal crystallization, a role that has also been observed before in crystallizations of other zeolites [35]. Control experiments on gels without TMA led to the crystallization of dense cristobalite phases in 10–30 days. This implies that TMA plays a role of structure-directing and promotes the formation of the GSQ framework structure, but not in the way forming a void-filled SDA/framework compound known for many SDAs or “templates” in zeolite syntheses. The TG/DTA of GSQ3 is presented in Figure S1 in the Supporting Information. In principle, the results are identical to those of GSQ4, with the same weight loss and heat effects, but slightly different weight changes and heat values because of the different amounts of the amorphous impurity. TMA is not present in GSQ3 sample, either.

Using  $[\text{GeO}_2]_{20}$ -AST as an example, Villaescusa and Cambor demonstrated that upon heating under oxygen deficiency in closed zeolite cages/channels, occluded organic species in the zeolite pores can reduce the framework Ge atoms, causing structural collapse. The residual germanium species can then be reoxidized to  $\text{GeO}_2$  and show weight gain in TG. With tetramethylammonium cation occluded in AST, the endothermic reduction of framework Ge occurs at approximately 500 °C, and the exothermic formation of  $\text{GeO}_2$  occurs at near 700 °C [36]. The phase changes in GSQ4 are hardly compatible with these processes. Even if TMA is present, the organo-reduction is unlikely to happen below 200 °C. The weight turbulences above 1000 °C are imputed to the buoyance due to the hot air (Figure 3a).

The  $^{29}\text{Si}$  MAS NMR spectra of samples GSQ1-GSQ4 are shown in Figure 4. They are of moderate resolutions with recognizable  $\text{Q}^4 \text{Si}-(\text{OSi})_4$  signal at -110 ppm and  $\text{Q}^3 \text{GeO-Si}-(\text{OSi})_3$  or  $\text{Q}^3 \text{HO-Si}-(\text{OSi})_3$  signal at -100 ppm. The resonance presenting at -82 ppm is coincident with the only Si species in the silicogermanate pharmacosiderite, i.e., a tetrahedral Si that is O-bonded to four octahedral Ge atoms [37]. Unfortunately, the spectra cannot be used to quantify these three species for

several reasons. (1) The presence of the amorphous impurity prevents the distinction between the Q3 and Q4 peaks for either phase. (2) The crystalline structure does not provide sufficient room for atmospheric, paramagnetic O<sub>2</sub> molecules to access and aid <sup>29</sup>Si spin-lattice relaxation. In this case, the 60 s delay time is far too short to generate spectra with a quantitative character [38]. There is no sign of resonances at approximately -210 ppm for SiO<sub>6</sub>-octahedra [39, 40]. Over all, “true” parmacosiderite with [GeO<sub>6</sub>]-octahedra exists, probably as domains within the GSQ framework. The presence of Q<sup>3</sup> is also likely to be attributed by broken connectivity, that is defects and structural distortions [41, 42].

The obtained materials do not contain fluorine. Neither XRF nor <sup>19</sup>F MAS NMR detected fluorine in any of the 4 samples, GSQ1-GSQ4. In the acidic gel, F is the species acting as the mineralizer to dissolve, transport and deposit the framework building blocks. In zeolites with small cages, F<sup>-</sup> ions can be trapped inside the cages during crystallization [33, 43]. F atoms can also be found in zeolite products with connectivity defects at the bond terminals in the form of -Si-F<sub>x</sub> [20, 44]. Neither occurred in the present products. GSQ does not contain small cages (elaborated below). The long crystallization time enables the complete hydrolysis of the terminal -Si-F<sub>x</sub> bonds.

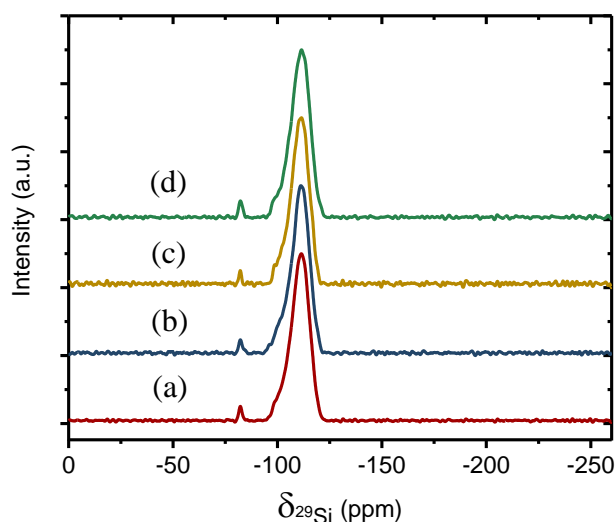


**Figure 4:** <sup>29</sup>Si MAS NMR spectra of the hydrothermal crystallization products from gels with increasing Ge/Si ratios as in Table 1, GSQ1-GSQ4 (a-d).

## Structure refinement

XRD shows great similarity between the GSQ and phramacosiderite phases. Elemental analysis and  $^{29}\text{Si}$  NMR results indicate that most of the octahedral Ge is missing and the Si atoms are not octahedrally coordinated.

Pawley fitting of the XRD histogram up to the resolution of  $1.2 \text{ \AA}$  ( $2\theta \sim 80^\circ$ ) converged with 48 (*hkl*) peaks in the refined unit cell with  $a = 7.696 \text{ \AA}$  (Table S1 in the Supporting Information). No systematic absence corresponds to the cubic space group P-43m (#215).

Shelx has proposed a framework with two distinct T-tetrahedra. T1 is located at  $x = y = z = \text{ca. } 0.36$ , with a four-fold multiplicity and site symmetry of 3m. T2 at the face center with a triple multiplicity and site symmetry of  $\bar{4}2m$ . The Q peak between the two T sites is assigned to the shared O atom. Another smeared Q at the cell center belongs to one leg of T1, with a distance of  $2.23 \text{ \AA}$ . It is more plausible to treat it as four -OH groups, considering the large displacement and unrealistically positive charge of the oxidic framework (Figure S2 in the Supporting Information). As a result, the framework is four-connected; however, T1 has an interruption, with one corner terminating as  $\equiv\text{T-O-H}$ . There are two additional Q peaks in the void spaces, which are assigned to the O atoms of the pore-filling  $\text{H}_2\text{O}$  molecules. The Shelx .res file is provided in the Supporting Information. A further concern in the model is that for the dangling -OH groups at T1, the available volume cannot accommodate all four of them with the modeled stretching directions simultaneously. It is logical to assume that they exist in partial occupancies and/or stretch in disordered directions to avoid short contacts. This concern is addressed by Rietveld refinement.

The Rietveld refinement conditions and results of the structural model against the experimental XRD data are listed in Table 2. The simulated XRD of the refined model and the experimental XRD are compared in Figure 5. The .cif file of the refined model is deposited in CCDC #2266230. The atomic coordinates and bond geometries are listed in Tables S2 and S3.

Table 2: Structural model and the experimental (Sample GSQ4) parameters for Rietveld refinement.

Wavelength (Å)	1.540510/1.544330 (Cu Kα)
Temperature (K)	298
2θ Range (°)	5-120 (7-118 used)
Step size (°)	0.01
No. of observations	11101
No. of variables	41
No. of reflections	95
Space group	P-43m (#215)
Unit cell parameter	
a (Å)	7.70049(13)
Cell volume (Å <sup>3</sup> )	456.621(23)
Residuals	
R <sub>wp</sub>	0.10306
R <sub>p</sub>	0.0723
R <sub>F</sub>	0.09259
Reduced $\chi^2$	1.53

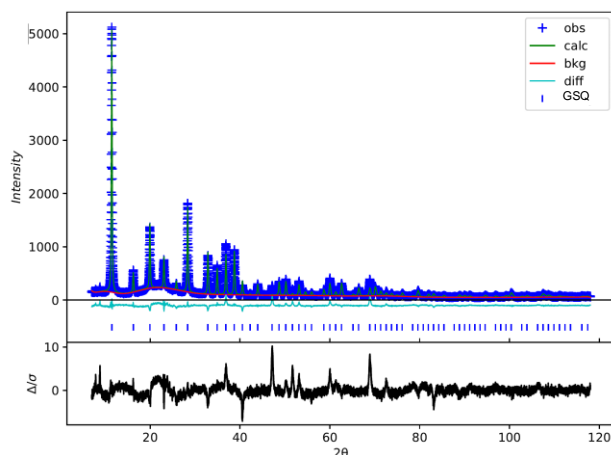


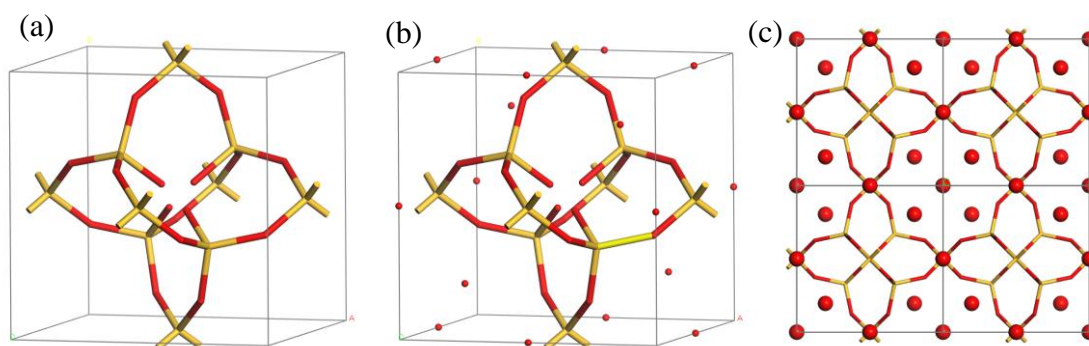
**Figure 5:** Experimental and refined XRD.

The basic unit of the structure is a branched chain of four tetrahedra: T1 is close to the cell center and radiates with three T2 in rectangular directions (Figure 6). Both tetrahedra are slightly larger than ideal SiO<sub>4</sub>, i.e., the one with Si–O length of approximately 1.6 Å and O–Si–O angle of approximately 109.5°. The four T–O lengths in T2 are equal and have a value of 1.6685 Å. The shape is slightly elongated in the direction parallel to the (100) plane, with O–Si–O angles of 112.52° along the cell edge and 103.54° perpendicular to the cell edge. T1 is more distorted. The T–O lengths are T1–O1 = 1.7016 Å long, T1–O3 (T1–O–H) = 1.5769 Å. O3 interrupts the

framework and terminates as -OH groups. It has a partial occupancy of 0.723 and a large thermal displacement of 0.408. Thus, the size and shape of the T1 tetrahedron are loose. The orientations of the -OH groups can be disordered. T–O–T bridges can form by missing the 0.277 fraction. Through these variations, short contacts of the O3 atoms with each other are avoided.

By a  $-43m$  operation, the piece of four tetrahedra further builds a propeller-shaped unit. In all directions, a 6-membered ring is observed. These rings possess dangling -O3-H groups pointing inside (Figure 6a).

The translation of the unit cell makes a three-dimensional 8-ring channel system, where H<sub>2</sub>O molecules reside (Figure 6b and 6c). Two positions for O atoms are discovered in the channels: one at the cell edge and the other at a four-fold position with partial occupancies. These positions are outside the range of short contacts with the framework atoms. Moreover, the thermal displacement values are large. It can be considered that the individual water molecules are displaced from these sites in disordered directions toward the framework, forming hydrogen bonds with the framework oxygen. Based on the TG and *in situ* XRD results, pore-filling H<sub>2</sub>O molecules are necessary to reinforce the distorted framework. H atoms almost do not contribute to X-ray scattering; thus, they are excluded from the modeling. The refined unit cell content was determined to be Si<sub>7</sub>O<sub>19.73</sub>. The composition of the material, including H atoms, is close to |(H<sub>2</sub>O)<sub>4.84</sub>|(SiO<sub>2</sub>)<sub>3</sub>(Si<sub>4</sub>O<sub>6</sub>(OH)<sub>2.89</sub>)]-GSQ. The total water content is approximately 17 wt%. TG shows a loss of approximately 15 wt %. Considering the framework charges and the discrepancy in water content, the



existence of impurities, intergrowths, and defects are revealed.

**Figure 6:** Framework (a), the unit cell (b), and the 8-ring channels filled with (water) oxygen (c) of refined GSQ.

### Structural similarity to pharmacosiderite

Figure 1c shows the experimental XRD pattern of sample GSQ4 compared to the simulated ones of the mineral pharmacosiderite-type titanosilicate (ICSD99628) [45], and its pure germanium counterpart (ICSD36523) [46]. Except for slightly different lattice distances, the XRD patterns appear identical.

Pharmacosiderite is a mineral family with an octahedron/tetrahedron-mixed framework. The type material is a ferroarsenate mineral  $K[Fe_4(OH)_4As_3O_{12}] \cdot 6 \sim 7H_2O$ , where 6-coordinated Fe ( $FeO_6$ -octahedron) builds up a central  $Fe_4(OH)_4O_{12}$  cluster that further links to four  $AsO_4$ -tetrahedra. Isomorphous substitutions of other elements for both O and T atoms make the pharmacosiderite family abundant in chemical composition and have provided the basis for more than 50 studies on crystal structure analyses [34].

We chose titanosilicate  $HK_3(TiO)_4(SiO_4)_3(H_2O)_4$ , ICSD99628[45] and pure germanate  $HK_3(Ge_7O_{16})(H_2O)_4$ , (ICSD36523)[46] to discuss the analogy of GSQ with pharmacosiderite. Figure 7 shows a unit cell model of potassium germanate, illustrating its framework and channels. The titanosilicate is isostructural. The model is shown in

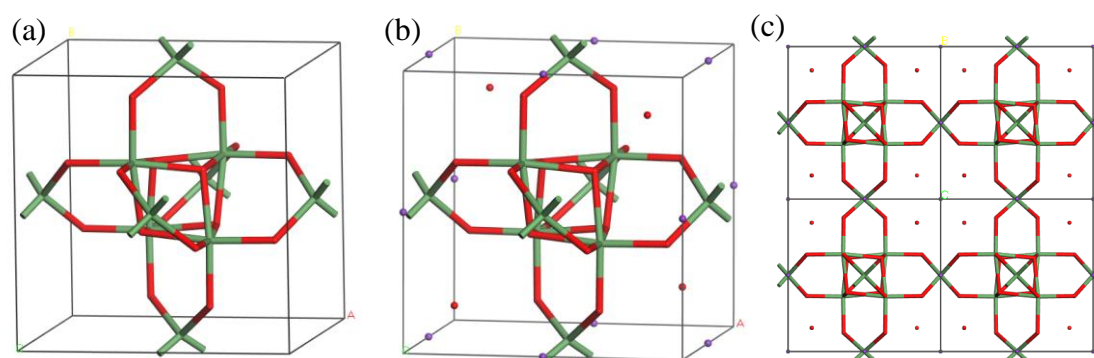


Figure S3 in the Supporting Information.

**Figure 7:** Potassium germanate  $HK_3(Ge_7O_{16})(H_2O)_4$ , (ICSD36523), of the pharmacosiderite structure: (a) the framework, (b) the unit cell, and (c) the channel

filled with hydrated  $K^+$  ions.

As shown in Figure 7, the framework of the germanate is centered on a  $[Ge_4O_4O_{12}]$ -unit, where the four Ge atoms in the 6-coordinated octahedra are linked by sharing four O atoms. Through the other 12 oxygen atoms, the center unit is further linked to six  $GeO_4$ -tetrahedra to build up a shape that is similar to the “propeller” of GSQ. A proton must exist in the center to hold the three-fold coordinated O atoms. The hydrated  $K^+$  ions in the 8-ring channels provide further charge balance. The  $GeO_4$ -tetrahedron takes the position of T2 in the GSQ but is more relaxed. The bond length of Ge–O in the tetrahedron is 1.76 Å, and the two values of O–Ge–O angles are 106.7 and 115.2°. The octahedron has Ge–O lengths of 1.84, and 1.97 Å. The O–Ge–O angles are in the range of 78–95°.

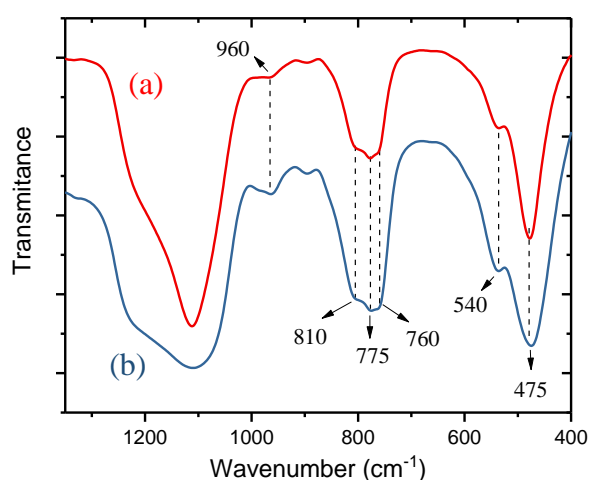
The difference between the GSQ framework and pharmacosiderite is that the four octahedra are substituted with four distorted tetrahedra. The four-connected framework interrupts this position with an–OH at each tetrahedron, but with partial occupancy and displacements. As Baur pointed out, the octahedron/tetrahedron-mixed pharmacosiderite framework is rigid [34]. Substitutions of different types of polyhedral units tends to cause large structural distortions, making the resulting material vulnerable to collapse.[34] This is indeed the case for GSQ. In pharmacosiderite, the “propeller” is made of 2-membered rings consisting two corner-sharing octahedra and 3-membered rings of two octahedra and one tetrahedron. These types of rings do not exist in GSQ. The “propeller” of GSQ contains only 6-rings of tetrahedra.

### **Role of germanium**

Germanium can form an octahedron with O atoms, whereas silicon is too small to stabilize the oxygen-built octahedron. The octahedron/tetrahedron-mixed pharmacosiderite framework is thermodynamically stable, whereas the four-connected GSQ is under great tension. Hence, it is logical to envisage that in the GSQ1-GSQ4 materials with increasing Ge content, Ge atoms are occasionally incorporated into the framework. It may take the place of T1 and form a  $GeO_6$ -octahedron, thus releasing the framework tension and making the real material to possess intergrown domains of

the “true” pharmacosiderite structure. It may also take T2 as a larger and deformed tetrahedron that relaxes the framework [47]. However, the material in general is definitely not a germanosilicate pharmacosiderite with the O/T-mixed framework. Rather, they have a four-connected structure, with only a small and non-stoichiometric portion of the built-in octahedra healing. As mentioned, the Ge/Si ratios of these materials are smaller than 0.15, which is far below the Ge/Si ratio of 4/3 required to form an O/T-mixed pharmacosiderite. We performed a control experiment with a starting gel of the same composition but with 0 content of GeO<sub>2</sub> (GSQ0 in Table 1). After 30 days at 160 °C, the gel did not crystallize. Healing through octahedron-incorporation is necessary for the crystallization of the material.

Figure 8 shows the FTIR spectra of GSQ3 and GSQ4. The absorption band at 475 cm<sup>-1</sup> belongs to the symmetric bending vibration  $\delta(\text{O-Si-O})$  and  $\delta(\text{O-Ge-O})$ , which is not distinguishable for either. The band between 700 and 900 cm<sup>-1</sup> is the symmetric bending of  $\delta(\text{Si-O-Si})$ ,  $\delta(\text{Ge-O-Ge})$ , or  $\delta(\text{Ge-O-Si})$  [48, 49]. The band contains multiple components and seems to evidence the existence of all these bonds. However, clear evidence for the Ge-O-Si bond is provided by the absorption at 960 cm<sup>-1</sup>, which belongs to the  $\nu(\text{Si-O})$  stretching with a directly linked heteroatom [50]. The strong band at 1100–1200 cm<sup>-1</sup> is the asymmetric stretching of  $\nu(\text{Si-O-Si})$  [48, 49]. The



peak at 540 cm<sup>-1</sup> corresponds to breathing of the zeolitic rings [49, 51-53]. An absorption band that can be definitely attributed to GeO<sub>6</sub>-octahedron at 485 cm<sup>-1</sup> is not resolved [37].

**Figure 8:** FTIR spectra of the samples GSQ3 (a) and GSQ4 (b) as in Table 1.

Concerning the charge balance of the oxidic framework, especially the incorporation of six-coordinated  $\text{GeO}_6$ -units that causes two negative charges at each site, we suspect that some  $\text{H}^+$  cations are exchangeable. Indeed, after soaking in 0.2 M NaCl solutions at 80 °C overnight,  $\text{Na}^+$  has been detected by XRF in all four samples GSQ1-GSQ4 (Table1). In all four samples, the Na/Ge ratios after the ion-exchange experiment are less than 1, and stoichiometry does not exist. This indicates that not all Ge atoms are present as octahedra, replacing the T1 sites. Ge may also be present at T2. The Ge content of the amorphous impurity may also affect the ion-exchange capacity.

Thus, the real material is the defective four-connected GSQ framework healed by the incorporation of pharmacosiderite domains; alternatively, from the other way of inspection, it is a pharmacosiderite with a significant deficiency of  $\text{GeO}_6$ -octahedra, where broken  $\text{SiO}_4$ -tetrahedra are taken as proxies.

## Conclusions

A germanosilicate named GSQ has crystallized in a strongly acidic and fluoride-containing medium. GSQ has a new four-connected framework structure analogous to the octahedron/tetrahedron-mixed framework of the pharmacosiderite family. The octahedra in the pharmacosiderite framework are replaced by  $\text{SiO}_3\text{OH}$  units, which makes the four-connected framework interrupted at this position. A small portion of the  $\text{GeO}_6$ -octahedra (eventually also  $\text{GeO}_4$ -tetrahedra) is occasionally incorporated to release the tension of the pure 4-connected framework. The refined unit cell of GSQ has a cubic symmetry, space group P-43m (#215), with  $a = 7.70049(13)$  Å. GSQ is vulnerable to heating and collapses above 200°C.

The chemical composition of the synthesis gel is simple. It contains  $\text{GeO}_2/\text{SiO}_2$  gels, HCl, and HF in water. Trimethylamine is a necessary organic additive for synthesis; however, it is not occluded in the framework voids of the product. TMA/HCl/HF in water forms a buffer that maintains the pH value of approximately 3 during the crystallization. In previous studies on zeolite synthesis in acidic media, we predicted that the discovery of new compositions and structures would be enabled by the expansion of zeolite crystallization chemistry into acidic fields [18-20]. Now, we

provide GSQ as a successful example to demonstrate the capability of this new chemistry.

However, the synthesis of zeolites in acidic media has not yet been explored. This study shows that synthesis in an acidic medium can deliver new structures even with simple amine additives. Therefore, acidic synthesis is a useful method for discovering new zeolites and is fundamentally different from the exploration of sophisticated organic structure-directing agents.

### **Author Contributions**

**G. Fu:** Investigation, Methodology, Writing – original draft. **Q. Lang, X. Liu, H. Zhao, Y. Sun, L. Zhao, A. Omran:** Investigation. **P. Lu:** Supervision. **X. Yang:** Conceptualization, Supervision, Methodology, Investigation, Writing – original draft. **B. Yu:** Supervision. **V. Valtchev:** Supervision, Writing – review & editing.

### **Conflicts of interest**

There are no conflicts to declare.

### **Acknowledgments**

The ZeoMat Group acknowledges the starting grant provided by QIBEBT, support provided by the Shandong Energy Institute (SEI S202107), and Nature Science Foundation of Shandong Province (ZR2022MB053 and ZR2022QB216). VV, XY, and PL acknowledge the collaboration under the Sino-French International Research Network (IRN) “Zeolites”.

### **Funding**

Shandong Energy Institute (SEI S202107), and the Nature Science Foundation of Shandong Province (ZR2022MB053 and ZR2022QB216).

### **References**

- [1] E.M. Flanigen, Molecular sieve zeolite technology - the first twenty-five years, *Pure & Appl. Chem.* 52 (1980) 21.
- [2] W. Vermeiren, J.P. Gilson, Impact of zeolites on the petroleum and petrochemical

- industry, *Topics in Catal.* 52 (2009) 1131-1161.
- [3] R.M. Milton, Molecular sieve science and technology, a historical perspective, in: M.L. Occelli, H.E. Robson(Eds.), *Zeolite Synthesis*, American Chemical Society, Washington DC, 1989, pp. 1-10.
- [4] A.J. Mallette, S. Seo, J.D. Rimer, Synthesis strategies and design principles for nanosized and hierarchical zeolites, *Nature Synth.* 1 (2022) 521-534.
- [5] Y. Li, L. Li, J. Yu, Applications of zeolites in sustainable chemistry, *Chem* 3 (2017) 928-949.
- [6] Y. Li, J. Yu, Emerging applications of zeolites in catalysis, separation and host-guest assembly, *Nature Rev. Mater.* (2021).  
<https://doi.org/10.1038/s41578-021-00347-3>.
- [7] M. Moliner, F. Rey, A. Corma, Towards the rational design of efficient organic structure-directing agents for zeolite synthesis, *Angew. Chem. Int. Ed.* 52 (2013) 13880-13889.
- [8] D. Schwalbe-Koda, S. Kwon, C. Paris, E. Bello-Jurado, Z. Jensen, E. Olivetti, T. Willhammar, A. Corma, Y. Román-Leshkov, M. Moliner, R. Gómez-Bombarelli, A priori control of zeolite phase competition and intergrowth with high-throughput simulations, *Science*, 374 (2021) 308-315.
- [9] J. Li, A. Corma, J. Yu, Synthesis of new zeolite structures, *Chem. Soc. Rev.* 44 (2015) 7112-7127.
- [10] R.F. Lobo, S.I. Zones, M.E. Davis, Structure-direction in zeolite synthesis, *J. inclusion phenom. and molec. recogn. in chem.* 21 (1995) 47-78.
- [11] Q.-F. Lin, Z.R. Gao, C. Lin, S. Zhang, J. Chen, Z. Li, X. Liu, W. Fan, J. Li, X. Chen, M.A. Camblor, F.-J. Chen, A stable aluminosilicate zeolite with intersecting three-dimensional extra-large pores, *Science*, 374 (2021) 1605-1608.
- [12] E. Kapaca, J. Jiang, J. Cho, J.L. Jordá, M.J. Díaz-Cabañas, X. Zou, A. Corma, T. Willhammar, Synthesis and structure of a  $22 \times 12 \times 12$  extra-large pore zeolite ITQ-56 determined by 3D electron diffraction, *J. Am. Chem. Soc.* 143 (2021) 8713-8719.
- [13] I. Rivin, A lesson from virtual zeolites, *Nature Mater.* 5 (2006) 931-932.
- [14] W. Chaikittisilp, T. Okubo, No more trial and error for zeolites, *Science*, 374 (2021) 257-258.
- [15] C. Baerlocher, L.B. McCusker, D.H. Olson, Database of zeolite structures, [www.iza-online.org](http://www.iza-online.org), 2023 (accessed 19 Nov. 2023).
- [16] M. Treacy, M. Forster, Atlas of Prospective Zeolite Structures, <http://www.hypotheticalzeolites.net/>, 2023 (accessed 19 Nov. 2023).
- [17] D. Shi, K.-G. Haw, C. Kouvatas, L. Tang, Y. Zhang, Q. Fang, S. Qiu, V. Valtchev, Expanding the synthesis field of high-silica zeolites, *Angew. Chem. Int. Ed.* 59 (2020) 19576-19581.
- [18] H. Zhao, Q. Lang, G. Fu, R. Ding, S. Wang, X. Yang, V. Valtchev, Hydrothermal crystallization of clathrasils in acidic medium: energetic aspects, *Micropo. Mesopo. Mater.* 333 (2022) 111728.
- [19] X. Yang, E. Dib, Q. Lang, H. Guo, G. Fu, J. Wang, Q. Yi, H. Zhao, V. Valtchev, Silicalite-1 formation in acidic medium: synthesis conditions and physicochemical properties, *Micropo. Mesopo. Mater.* 329 (2022) 111537.
- [20] G. Fu, E. Dib, Q. Lang, H. Zhao, S. Wang, R. Ding, X. Yang, V. Valtchev, Acidic medium synthesis of zeolites – an avenue to control the structure-directing power of organic templates, *Dalton Trans.* 51 (2022) 11499-11506.
- [21] Q. Lang, G. Fu, H. Zhao, J. Wang, X. Yang, V. Valtchev, Biomineralization at the molecular level: amino acid-assisted crystallization of zeotype  $\text{AlPO}_4 \cdot 1.5\text{H}_2\text{O} \cdot \text{H}_3$ , *Crystal Growth & Design*, 21 (2021) 7298-7305.

- [22] C.S. Cundy, P.A. Cox, The Hydrothermal synthesis of zeolites: history and development from the earliest days to the present time, *Chem. Rev.* 103 (2003) 663-702.
- [23] D.W. Breck, *Zeolite molecular sieves: structure, chemistry, and use*, John Wiley and Sons, New York, London, Sydney, and Toronto, 1974.
- [24] P. Caullet, J.-L. Paillaud, A. Simon-Masseron, M. Soulard, J. Patarin, The fluoride route: a strategy to crystalline porous materials, *Comptes Rendus Chimie*, 8 (2005) 245-266.
- [25] M.A. Cambor, L.A. Villaescusa, M.J. Díaz-Cabañas, Synthesis of all-silica and high-silica molecular sieves in fluoride media, *Topics in Catal.* 9 (1999) 59-76.
- [26] P.-E. Werner, L. Eriksson, M. Westdahl, TREOR, a semi-exhaustive trial-and-error powder indexing program for all symmetries, *J Appl. Crystallography* 18 (1985) 367-370.
- [27] A. Altomare, C. Cuocci, C. Giacovazzo, A. Moliterni, R. Rizzi, N. Corriero, A. Falcicchio, EXPO2013: a kit of tools for phasing crystal structures from powder data, *J. Appl. Crystallography*, 46 (2013) 1231-1235.
- [28] G. Sheldrick, A short history of SHELX, *Acta Crystallographica Section A*, 64 (2008) 112-122.
- [29] B.H. Toby, R.B. Von Dreele, GSAS-II: the genesis of a modern open-source all purpose crystallography software package, *J. Appl. Crystallography*, 46 (2013) 544-549.
- [30] M.H. Mendenhall, K. Mullen, J.P. Cline, An implementation of the fundamental parameters approach for analysis of X-ray powder diffraction line profiles, *J. Res. National Institute of Standards and Technology*, 120 (2015) 223-251.
- [31] X.B. Yang, Synthesis and crystal structure of tetramethylammonium fluoride octadecasil, *Materials Research Bulletin*, 41 (2006) 54-66.
- [32] X. Yang, B.H. Toby, M.A. Cambor, Y. Lee, D.H. Olson, Propene adsorption sites in zeolite ITQ-12: a combined synchrotron X-ray and neutron diffraction study, *J. Phys. Chem. B* 109 (2005) 7894-7899.
- [33] X. Yang, M.A. Cambor, Y. Lee, H. Liu, D.H. Olson, Synthesis and crystal structure of As-synthesized and calcined pure silica zeolite ITQ-12, *J. Am. Chem. Soc.* 126 (2004) 10403-10409.
- [34] W.H. Baur, Rigid frameworks of zeolite-like compounds of the pharmacosiderite structure-type, *Micropo. Mesop. Mater.* 151 (2012) 13-25.
- [35] X.B. Yang, X.Y. Zhao, J.M. Xiao, Q. Fan, R.N. Yang, L. Yu, High silica zeolite phi, a CHA type zeolite with ABC-D6R stacking faults, *Micropo. Mesop. Mater.* 248 (2017) 129-138.
- [36] L.A. Villaescusa, M.A. Cambor, Framework reduction of GeO<sub>2</sub> zeolites during calcination, *Chem. Mater.* 28 (2016) 7544-7550.
- [37] S. Feng, M. Tsai, S.P. Szu, M. Greenblatt, Preparation, characterization, and ionic conductivity of novel crystalline, microporous silicogermanates, *Chem. Mater.* 4 (1992) 468-472.
- [38] D.J. Cookson, B.E. Smith, Atmospheric oxygen as the dominant source of <sup>29</sup>Si spin-lattice relaxation in solid silicalite, *J. Magn. Resonance* (1969), 63 (1985) 217-218.
- [39] T.L. Weeding, B.H.W.S. de Jong, W.S. Veeman, B.G. Aitken, Silicon coordination changes from 4-fold to 6-fold on devitrification of silicon phosphate glass, *Nature*, 318 (1985) 352-353.
- [40] R. Dupree, D. Holland, M.G. Mortuza, Six-coordinated silicon in glasses, *Nature*,

328 (1987) 416-417.

- [41] D.H. Brouwer, J. Van Huizen, NMR crystallography of zeolites: how far can we go without diffraction data?, *Magn. Resonance in Chem.* 57 (2019) 167-175.
- [42] C.A. Fyfe, J.H. O'Brien, H. Strobl, Ultra-high resolution  $^{29}\text{Si}$  MAS NMR spectra of highly siliceous zeolites, *Nature*, 326 (1987) 281-283.
- [43] H. Koller, A. Wölker, L.A. Villaescusa, M.J. Díaz-Cabañas, S. Valencia, M.A. Cambor, Five-coordinate silicon in high-silica zeolites, *J. Am. Chem. Soc.* 121 (1999) 3368-3376.
- [44] Z.S. Lin, D. Chen, H.-Y. Nie, Y.T.A. Wong, Y. Huang, Investigations of the formation of zeolite ZSM-39 (MTN), *Canadian J. Chem.* 97 (2019) 840-847.
- [45] A. Tripathi, D.G. Medvedev, J. Delgado, A. Clearfield, Optimizing Cs-exchange in titanosilicate with the mineral pharmacosiderite topology: framework substitution of Nb and Ge, *J. Solid State Chem.* 177 (2004) 2903-2915.
- [46] R. Bialek, V. Grämlich, The superstructure of  $\text{K}_3\text{HGe}_7\text{O}_{16}\cdot 4\text{H}_2\text{O}$ , *Zeitschrift für Kristallographie - Cryst. Mater.* 198 (1992) 67-78.
- [47] X. Yang, D. Albrecht, J. Caro, Solvothermal synthesis of germanosilicate-sodalite and silica-sodalite: Effects of water, germanium and fluoride, *Micropo. Mesopo. Mater.* 100 (2007) 95-102.
- [48] E.M. Flanigen, H. Khatami, H.A. Szymanski, Infrared structural studies of zeolite frameworks, in: E.M. Flanigen, L. B. Sand (Eds.), *Molecular Sieve Zeolites-I*, American Chemical Society, Washington DC, 1974, pp. 201-229.
- [49] G. Coudurier, C. Naccache, J.C. Védrine, Uses of i.r. spectroscopy in identifying ZSM zeolite structure, *J. Chem. Soc., Chem. Commun.* (1982) 1413-1415.
- [50] G. Tozzola, M.A. Mantegazza, G. Ranghino, G. Petrini, S. Bordiga, G. Ricchiardi, C. Lamberti, R. Zulian, A. Zecchina, On the structure of the active site of Ti-silicalite in reactions with hydrogen peroxide: a vibrational and computational study, *J. Catal.* 179 (1998) 64-71.
- [51] S.L. Burkett, M.E. Davis, Mechanisms of structure direction in the synthesis of pure-silica zeolites. 1. synthesis of TPA/Si-ZSM-5, *Chem. Mater.* 7 (1995) 920-928.
- [52] S.L. Burkett, M.E. Davis, Mechanism of structure direction in the synthesis of Si-ZSM-5: an investigation by intermolecular  $^1\text{H}$ - $^{29}\text{Si}$  CP MAS NMR, *J. Phys. Chem.* 98 (1994) 4647-4653.
- [53] P.A. Jacobs, E.G. Derouane, J. Weitkamp, Evidence for X-ray-amorphous zeolites, *J. Chem. Soc., Chem. Commun.* (1981) 591-593.